Chapter 5: Heterolytic Activation of H_2 with an L_3Fe-(μ-N)-FeL_3 Linkage: Characterization of a Diiron System Featuring a (μ-NH), (μ-H) Manifold

5.1 Introduction

The interaction of dinitrogen-derived, surface-bound nitrides with H_2 is likely responsible for ammonia production during turnover in Haber-Bosch catalysis.[1] Despite this mechanistic postulate, the chemistry of iron compounds featuring either terminal[2] or bridging[3] nitride ligands has been slow to develop, and no system has been reported to react with H_2.[4]

Previous work in our laboratory established that the terminal iron(III) imide, $[PhBP_3]Fe{\equiv}N$-*p*-tolyl (**2.5**), is capable of complete H_2-induced Fe-N bond scission at room temperature to yield free *p*-toluidine.[5] Encouraged by this reactivity, we prepared a bridging nitride species, $[([PhBP_3]Fe)_2N][Na(THF)_5]$ (**4.2**), whose synthesis and ammonia production in the presence of excess protons has been established.[6] Herein we wish to report on the facile heterolysis of H_2 with **4.2** under mild conditions (room temperature, 1 atm H_2). The resulting imide-hydride product, $[([PhBP_3]Fe)_2(\mu\text{-}NH)(\mu\text{-}H)][Na(THF)_5]$ (**5.1**), is itself unique in that it represents the first example of a bimetallic system bridged exclusively by these two ligands.[7,8]

5.2 Results and Discussion

Incubation of a brown THF solution of **4.2** with an atmosphere of H_2 at room temperature results in a color change to green within minutes. Isolation and characterization of the resulting product demonstrated that a formal 1,2 addition process of H_2 had occurred to yield the bridging imide-hydride species, $[([PhBP_3]Fe)_2(\mu\text{-}NH)(\mu\text{-}H)][Na(THF)_5]$ (**5.1**) (Eq 5.1). Akin to nitride precursor **4.2**, compound **5.1** features a diamagnetic manifold and was conveniently characterized by ^{1}H, ^{31}P, and ^{15}N NMR

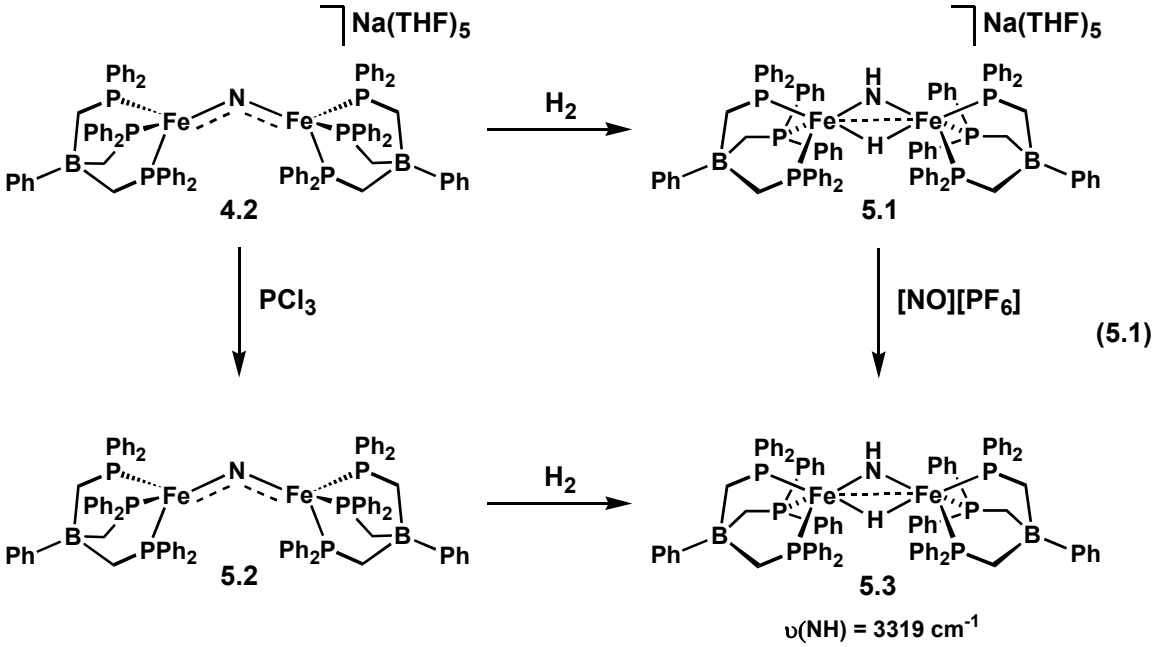

spectroscopy. The ^{31}P NMR spectrum exhibits a singlet at δ 66 ppm, which is 8 ppm downfield from the resonance observed for **4.2**. The ^{1}H NMR spectrum features singlet resonances at δ +18.5 and -22.4 ppm for the (μ-N*H*) and (μ-*H*) ligands, respectively, which are absent when **4.2** is hydrogenated with D_2. For the ^{15}N NMR experiment, **5.1**-(50% ^{15}N) was prepared from the hydrogenation of **4.2**-(50% ^{15}N) (δ 801 ppm (s)) and features a doublet at δ 406 ppm ($^{1}J_{N\text{-}H}$ = 63 Hz) (Figure 5.1A). This chemical shift and $^{1}J_{N\text{-}H}$ coupling constant are similar to those observed for the imide ligands of $(Cp^{*}Ti)_3(\mu\text{-}NH)_3(\mu\text{-}N)$ (δ 470 ppm, $^{1}J_{N\text{-}H}$ = 63 Hz).[9] The ^{1}H NMR spectrum of **5.1**-(50% ^{15}N) also exhibits a virtual triplet for the (μ-N*H*) resonance (Figure 5.1C), which is composed of a singlet from naturally abundant ^{14}N (I = 1) and a doublet from the ^{15}N label (I = 1/2). The (μ-*H*) resonance is unaffected by nitrogen labeling (Figure 5.1B).

When an isolated sample of **4.2** is exposed to an atmosphere of D_2, the hydride ligand undergoes deuterium exchange much more rapidly than the imide ligand. Thus on an NMR scale, the protio-hydride resonance is observed to fully decay within a few hours

of exposure to D_2 . The protio-imide resonance also decays at a noticeable rate, though it is still detectable after 3 days. One plausible mechanistic scenario for isotope exchange involves the oxidative addition of D_2 to a single iron center to form an iron(IV) bis-deuteride, mono-hydride intermediate. Hydride exchange would then result from reductive elimination of HD. Isotopic exchange at the imide ligand may be envisioned through an additional protonation/deprotonation event that precedes the reductive elimination step. It is worth noting that iron(IV) tri-hydride species supported by the second generation [PhB^{iPr}_3] ligand have been reported.[10]

Infrared spectroscopy of **5.1** failed to reveal any vibrations associated with either the imide or hydride ligands, regardless of how the sample was prepared for analysis (*i.e.*, THF solution, KBr pellet, or Nujol mull).

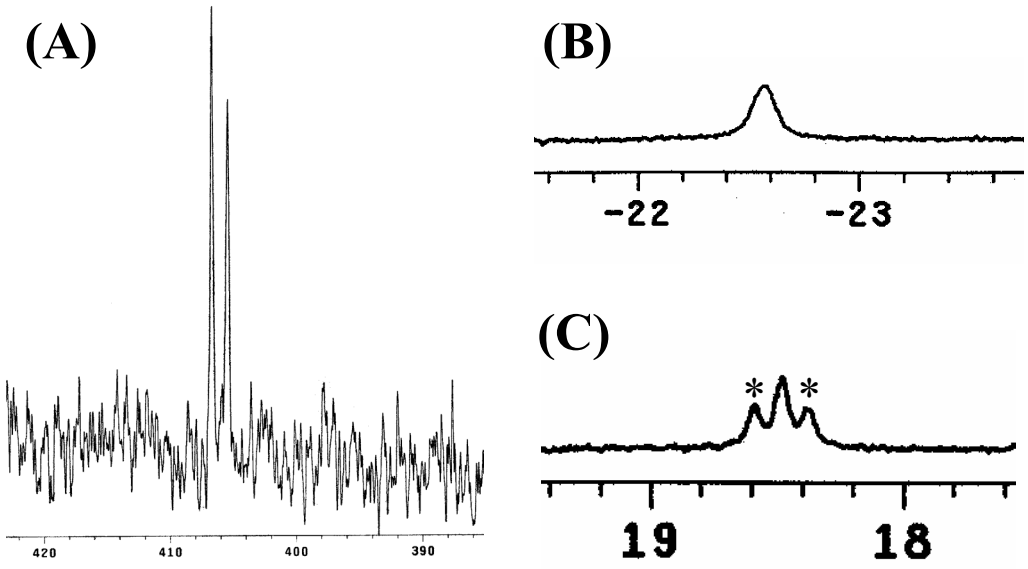

Figure 5.1. (A) Proton coupled ^{15}N NMR spectrum of **5.1**-(50% ^{15}N). (B) μ-H resonance observed in the ^{1}H NMR spectrum of **5.1**-(50% ^{15}N). (C) μ-NH resonance observed in the ^{1}H NMR spectrum of **5.1**-(50% ^{15}N). Peaks marked with an asterisk are due to coupling with the ^{15}N nuclei.

Crystals of **5.1** suitable for an X-ray diffraction experiment were grown via a THF/hexanes diffusion chamber, and the resulting solid state structure is shown in Figure 5.2. Although the imide-hydride bridge between Fe1 and Fe2 is disordered over two positions as a result of the two ligands flipping positions randomly throughout the crystal, electron density attributable to both the imide hydrogen and hydride ligands was located in the difference map and successfully refined when the Fe-H distances were constrained to be equal. Despite this disorder, the structure of **5.1** was of sufficient quality to establish the connectivity of the diiron core and provide reliable structural data concerning the more populated position of the Fe-(μ-NH)-Fe linkage (~ 70% occupancy). In comparison with nitride **4.2,** the Fe-N bond lengths for **5.1** have increased on average 0.118 Å (Fe-N = 1.675(5) Å, 1.705(5) Å for **4.2**; 1.790(5) Å, 1.826(5) Å for **5.1**), which is consistent with the loss of a bond order between the Fe-N linkages. The Fe-P bond distances of ~ 2.2 Å are similar to those of **4.2** while the Fe-N_x-Fe bond angle contracts from 135.9(3)° to 94.7(3)° upon addition of H_2. An iron-iron bonding interaction is required for the observation of a diamagnetic manifold and is evidenced by the relatively short Fe-Fe bond distance of 2.6588(9) Å. This value is approximately 0.45 Å shorter than that for **4.2** and is similar to the iron-iron distances observed in hydrogenase model compounds.[11]

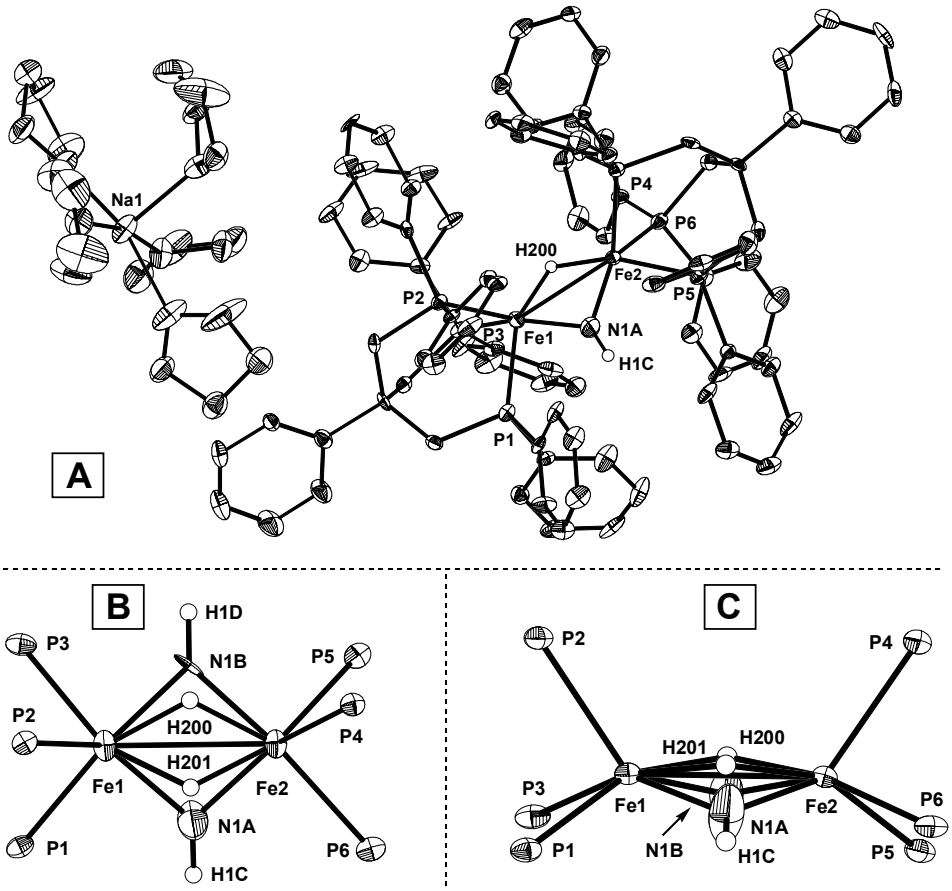

Figure 5.2. (A) 50% thermal ellipsoid representation of $[([PhBP_3]Fe)_2(\mu\text{-NH})(\mu\text{-H})][Na(THF)_5]$ **5.1** showing only the more populated position of the disordered (μ-NH)(μ-H) linkage. Selected bond distances (Å) and angles (°): Fe1-N1A: 1.826(5); Fe2-N1A: 1.790(5); Fe1-H200: 1.508(14); Fe2-H200: 1.508(14); Fe1-Fe2: 2.6595(9); Fe1-P1: 2.2121(13); Fe1-P2: 2.2024(13); Fe1-P3: 2.2274(13); Fe2-P4: 2.2247(13); Fe2-P5: 2.2306(13); Fe2-P6: 2.2411(13); Fe1-N1A-Fe2: 94.7(3); P1-Fe1-P2: 88.98(5): P1-Fe1-P3: 90.62(5); P2-Fe1-P3: 88.91(5); P2-Fe1-N1A: 125.5(2); P1-Fe1-N1A: 85.77(18); P3-Fe1-N1A: 145.2(2). (B) Top view of the L_3Fe-(μ-NH)(μ-H)-FeL_3 core of **5.1** showing both positions of the disordered (μ-NH)(μ-H) linkage. (C) Side view of the L_3Fe-(μ-NH)(μ-H)-FeL_3 core of **5.1** showing both positions of the (μ-NH)(μ-H) linkage.

The comparative cyclic voltammetry of **5.1** and **4.2** is shown in Figure 5.3. The electrochemical response for **5.1** features an irreversible oxidation at -0.15 V and two fully reversible redox events at -1.25 V and -2.58 V (vs. Fc/Fc^+). The event at -1.25 V is assigned to an $Fe(II)Fe(II)^-/Fe(II)Fe(III)$ redox process, which is similar to what has been proposed for **4.2** (-1.3 V vs. Fc/Fc^+).[6] That both **4.2** and **5.1** may be chemically oxidized by one electron (Eq 5.1) to yield $([PhBP_3]Fe)_2(\mu\text{-}N)$ (**5.2**) and $([PhBP_3]Fe)_2(\mu\text{-}NH)(\mu\text{-}H)$ (**5.3**), respectively, is consistent with this assignment. The irreversible oxidations at ~ -150 (**5.1**) and -350 mV (**4.2**) may correspond to an Fe(III)/Fe(IV) redox event at a single iron center, to an $Fe(III)Fe(II)/Fe(III)Fe(III)^+$ redox process, or to oxidative degradation of a borate ligand.[12] The reduction waves at low potential (-2.5 V for **4.2**, -2.6 for **5.1**) are interesting and are not observed in the iron imide systems. These events are suggestive of an $Fe(II)Fe(II)^-/Fe(II)Fe(I)^{2-}$ redox process that is fully reversible for **5.1**; for **4.2** the anodic wave decreases in intensity and eventually vanishes when this redox event is isolated and cycled multiple times. The chemical reduction of both **4.2** and **5.1** with an excess of sodium mirror yields a number of diamagnetic products as evidenced by ^{31}P NMR spectroscopy.

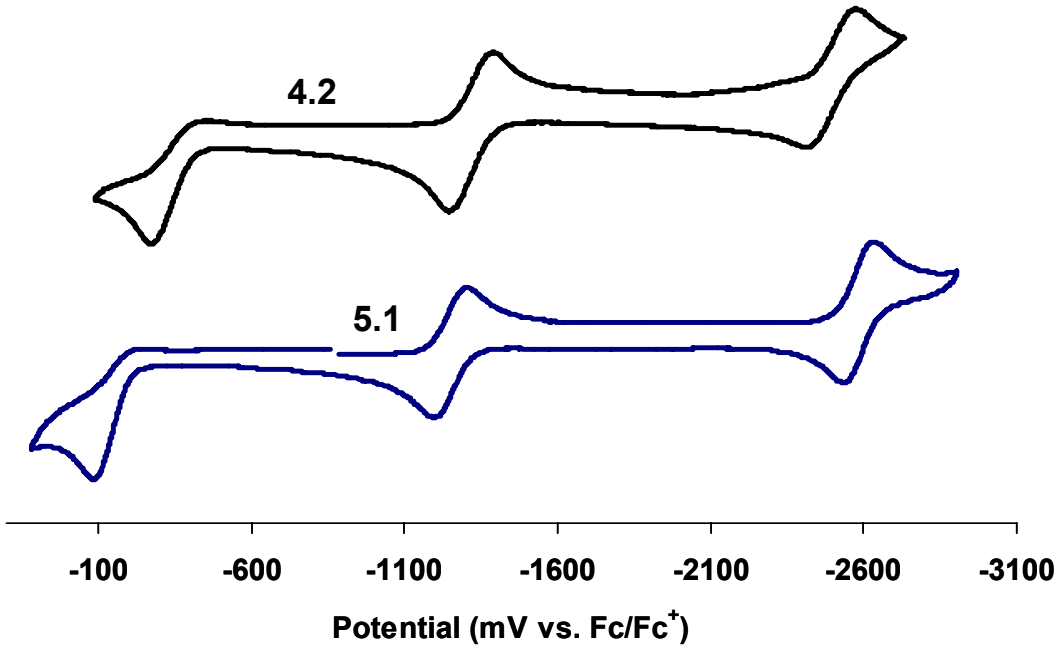

Figure 5.3. Cyclic voltammetry of [{[$PhBP_3$]Fe}$_2$(μ-N)][Na(THF)$_5$] (**4.2**), top, and [([$PhBP_3$]Fe)$_2$(μ-NH)(μ-H)][Na(THF)$_5$] (**5.1**), bottom. Experimental parameters: 2.0 mM analyte, 0.30 M [^{n}Bu$_4$N][PF_6] electrolyte, scan rate = 50 mV/s.

Crystals of **5.2** suitable for an X-ray diffraction experiment were grown via vapor diffusion of petroleum ether into a THF solution, and the resulting solid-state structure is shown in Figure 5.4. In contrast to parent nitride **4.2**, no disorder was observed for the nitride ligand as it was satisfactorily refined in one position. Structurally, the Fe-N bond lengths of 1.668(2) Å and 1.683(2) Å are virtually identical to each other and are similar to those observed for anionic **4.2** (see Table 5.1). Also apparent is the increase in linearity from 135.9(3)° to 142.4(1)° for the Fe-N-Fe manifold of the oxidized species. Consistent with the observation of iron-phosphorus bond expansion in going from the closed shell

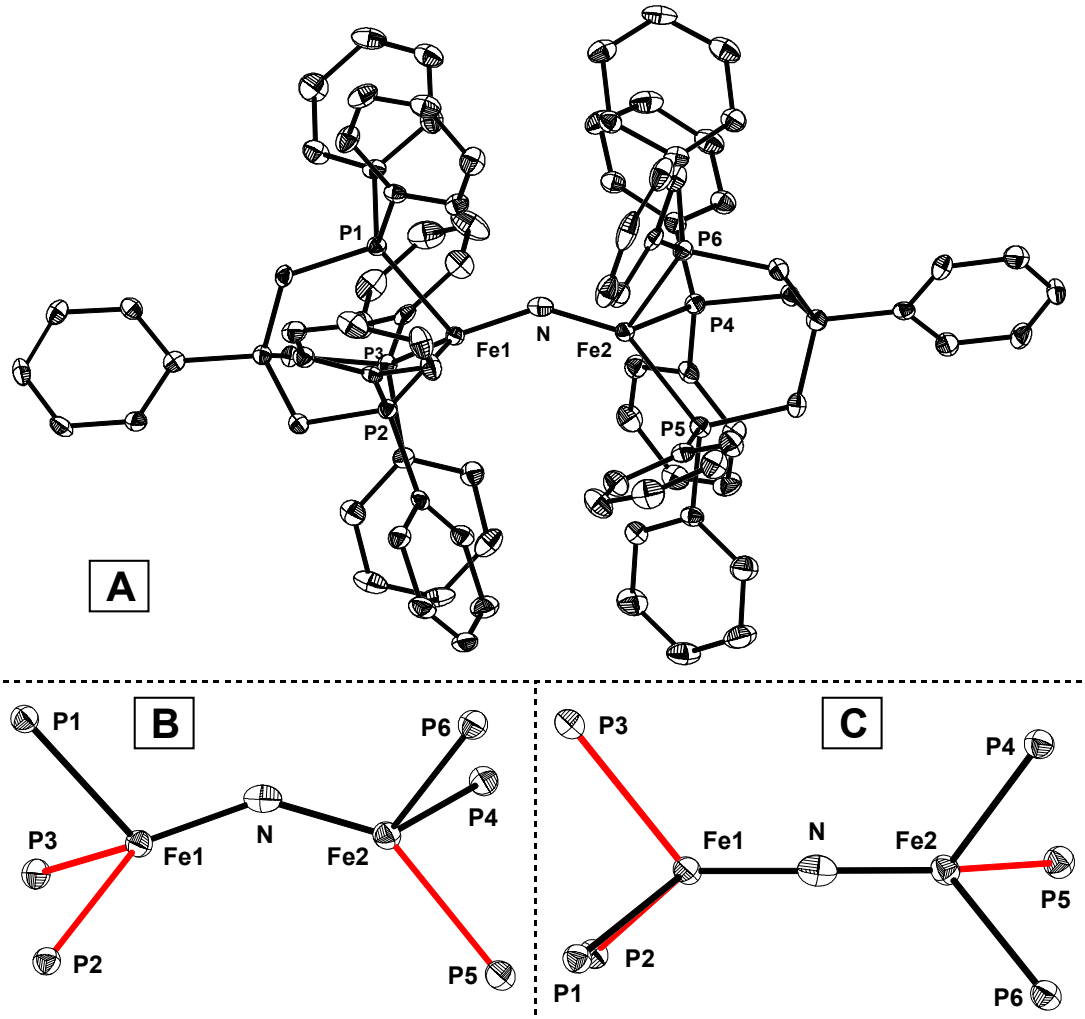

Figure 5.4. (A) 50% thermal ellipsoid representation of $([PhBP_3]Fe)_2(\mu\text{-}N)$ **5.2.** Two molecules of THF have been removed for clarity. Selected bond distances (Å) and angles (°): Fe1-N: 1.683(2); Fe2-N: 1.668(2); Fe1-Fe2: ~ 3.18; Fe1-P1: 2.2491(8); Fe1-P2: 2.3398(8); Fe1-P3: 2.3122(8); Fe2-P4: 2.2016(8); Fe2-P5: 2.3479(8); Fe2-P6: 2.2275(8); Fe1-N-Fe2: 142.41(12); P1-Fe1-P2: 88.37(3): P1-Fe1-P3: 88.45(3); P2-Fe1-P3: 94.03(3); P2-Fe1-N: 134.60(7); P1-Fe1-N: 111.76(7); P3-Fe1-N: 125.35(7). (B) Side view of the $L_3Fe\text{-}(\mu\text{-}N)\text{-}FeL_3$ core of **5.2**. (C) Top view of the $L_3Fe\text{-}(\mu\text{-}N)\text{-}FeL_3$ core of **5.2**. For both B and C, elongated Fe-P bonds are represented in red.

(d^6) to the open shell (d^5) iron imides, **5.2** features two elongated Fe-P bonds on Fe1 (2.3122(8) Å and 2.3398(8) Å vs. 2.2491(8) Å) and one elongated Fe-P bond on Fe2 (2.3479(8) Å vs. 2.2016(8) Å and 2.2275(8) Å). Whether this is an inherent property of the metalloradical systems, or the result of decreased back-bonding into σ^* orbitals of the [$PhBP_3$] ligand,[13] is still a matter of debate.[14] That both metal centers in **5.2** feature elongated Fe-P bonds suggests that the SOMO is delocalized over the entire L_3Fe-(μ-N)-FeL_3 linkage. Structural parameters for **4.2**, **5.1**, and **5.2** are summarized in Table 5.1.

Table 5.1. Structural data for compounds [([$PhBP_3$]Fe)$_2$(μ-N)][Na(THF)$_5$] (**4.2**), [([$PhBP_3$]Fe)$_2$(μ-NH)(μ-H)][Na(THF)$_5$] (**5.1**), and ([$PhBP_3$]Fe)$_2$(μ-N) (**5.2**).

Compound	d Fe-N_x (Å)	d Fe-P (Å)	d Fe-Fe (Å)	Angle Fe-N_x-Fe
[([$PhBP_3$]Fe)$_2$N][Na(THF)$_5$] (**4.2**)[a]	1.675(5)	2.2295(10) 2.2338(10) 2.2127(10)	~ 3.13	135.9(3)
Formal oxidation states: Fe(II)Fe(II)	1.705(5)	2.2299(10) 2.2106(10) 2.2534(10)		
[([$PhBP_3$]Fe)$_2$(μ-NH)(μ-H)][Na(THF)$_5$] (**5.1**)[a]	1.826(5)	2.2121(13) 2.2024(13) 2.2274(13)	2.6595(9)	94.7(3)
Formal oxidation states: Fe(II)Fe(II)	1.790(5)	2.2247(13) 2.2306(13) 2.2411(13)		
([$PhBP_3$]Fe)$_2$N (**5.2**)	1.683(2)	2.2491(8) 2.3398(8) 2.3122(8)	~ 3.18	142.41(12)
Formal oxidation states: Fe(II)Fe(III)	1.668(2)	2.2016(8) 2.3479(8) 2.2275(8)		

[a] Structural data are tabulated for the more populated position of the bridging linkage.

X-band EPR analysis of **5.2** at 4 K (Figure 5.5) reveals an axial signal that is consistent with the presence of one unpaired electron.[15] Also present is a weak, low-field signal ($g \sim 10.1$) that suggests **5.2** is best described electronically as a ground-state doublet arising from antiferromagnetic exchange between high-spin Fe(II) and Fe(III) nuclei. The extensive coupling observed for the axial signal likely arises from super-hyperfine coupling of the unpaired electron with multiple phosphorus nuclei (^{31}P: 100% abundance, $I = ½$), and possibly with the nitride ligand (^{15}N: 0.365% abundance, $I = ½$; ^{14}N: 99.635% abundance, $I = 1$).

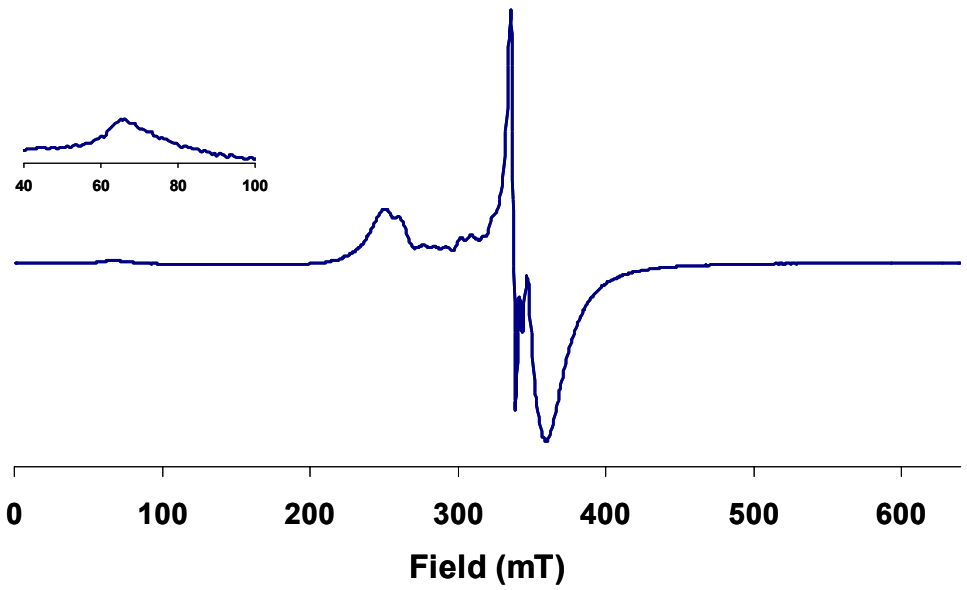

Figure 5.5. X-band EPR spectrum of $([PhBP_3]Fe)_2(\mu\text{-}N)$ (**5.2**) (glassy toluene, 4 K, 9.378 GHz). (*inset*) Region from 40–100 mT highlighting the low-field signal.

Solid-state magnetic susceptibility data for **5.2** were obtained from 4 to 300 K by SQUID magnetometry and are plotted, per dimeric unit, in Figure 5.6. The plot of μ_{eff} versus temperature (Figure 5.6 *top*) is consistent with antiferromagnetic coupling as μ_{eff} decreases upon cooling of the sample. A maximum value of 3.40 μ_B is observed at 300 K, which suggests that a fraction of the molecules are populating higher spin-states[16] as this value is considerably larger than the spin-only value for one unpaired electron (1.79 μ_B). At approximately 165 K, the μ_{eff} value of 2.52 μ_B begins to reflect that expected for one unpaired electron. A final value of 1.82 μ_B is obtained at 4 K, which is consistent with the ground-state doublet observed by EPR spectroscopy.

A plot of χ_M versus T (Figure 5.6 *bottom*) demonstrates that the antiferromagnetic exchange in **5.2** is weak. As shown in the inset, a slight increase and then a decrease in χ_M is observed as the sample is cooled from 300 to 185 K.[17] Although attempts to extract a *J* value for **5.2** from this data have thus far been unsuccessful, the relative magnitudes observed for **5.2** and **4.2** ($| J | \geq 250$ cm^{-1})[6] are intriguing considering the minimal structural differences observed between the Fe-N-Fe linkages. Geometrical considerations suggest that a larger coupling constant should be observed for the more linear Fe-N-Fe linkage of **5.2** as a result of better π-orbital overlap.[18] Such a trend is typically observed for bridging iron oxos,[19] although exceptions are known.[20] One plausible explanation for the present system is that the reduced symmetry of **5.2** (C_1) versus **4.2** (C_{2v}) alters the σ and π-bonding character of the Fe-N-Fe linkage in such a manner as to yield similar structural parameters but weaker π-orbital overlap.[21]

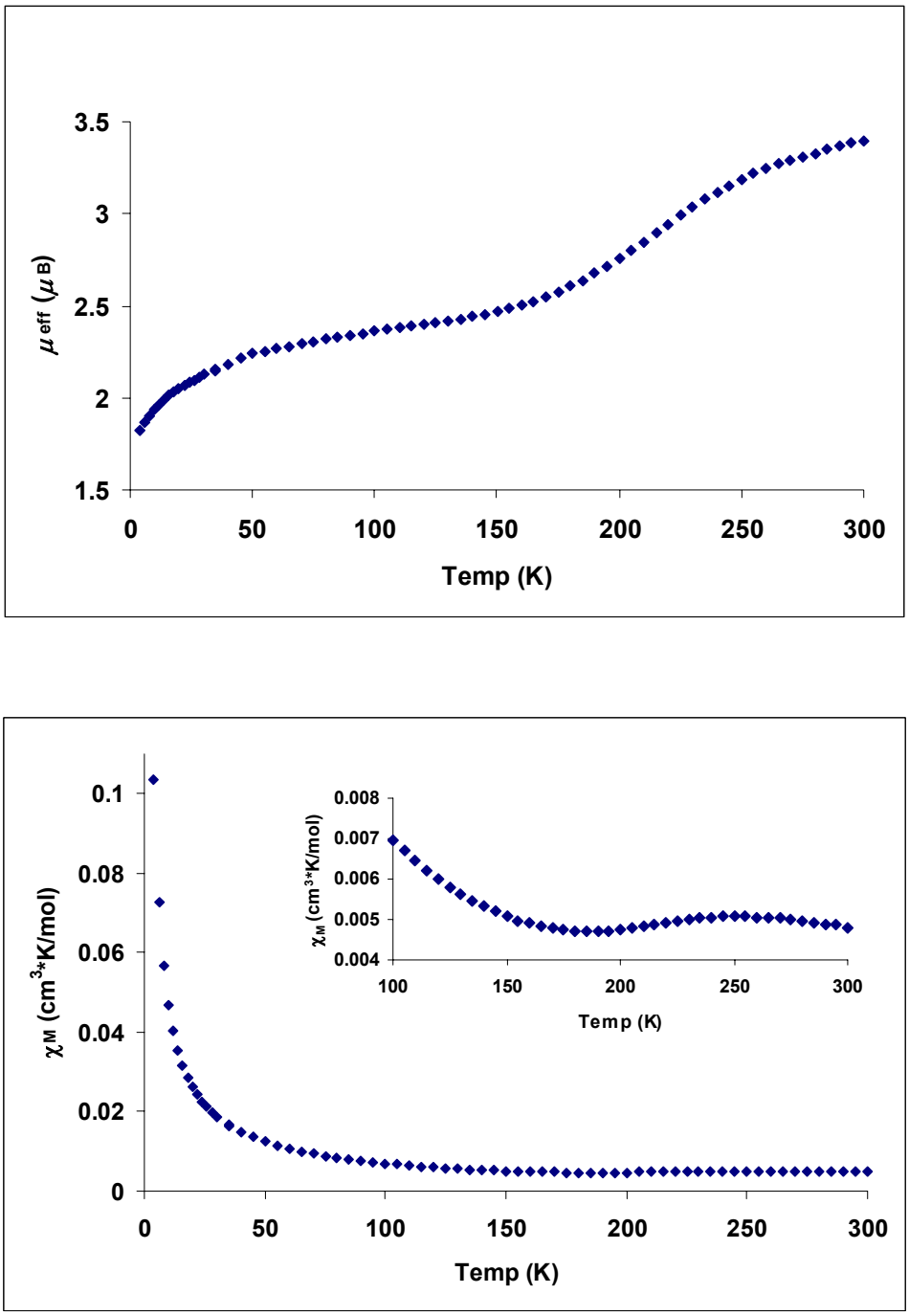

Figure 5.6. SQUID magnetometry data for $([PhBP_3]Fe)_2(\mu\text{-N})$ (**5.2**) plotted *per dimeric unit* as (*top*) μ_{eff} versus temperature and (*bottom*) $\chi_M T$ versus temperature. (*inset*) Plot of $\chi_M T$ versus temperature highlighting the region from 100–300 K.

The low-energy d-d electronic transitions centered at 1266 nm in the NIR spectrum of diamagnetic **4.2** cemented its assignment as an antiferromagnetically coupled, high-spin system.[6] For **5.2** these transitions are anticipated to blue-shift as a result of the increased oxidation state of the molecule.[22] Comparative optical data are therefore of interest and are shown in Figure 5.7. Upon initial inspection it becomes apparent that the low-energy features observed for **4.2** are absent in **5.2**. Present in the spectrum for **5.2** is a shoulder at ~ 650 nm and a broad feature that begins at ~ 1100 nm, which may correspond to the low-energy charge-transfer and d-d transitions, respectively, of **4.2**. Coincidently, the feature at 650 nm is of the same energy that is observed for the lower-energy charge-transfer bands of the iron(III) imides (See Chapter 2). The features at ~ 1370 nm in both spectra are instrumental artifacts and have been observed in a number of NIR spectrum acquired under similar conditions.

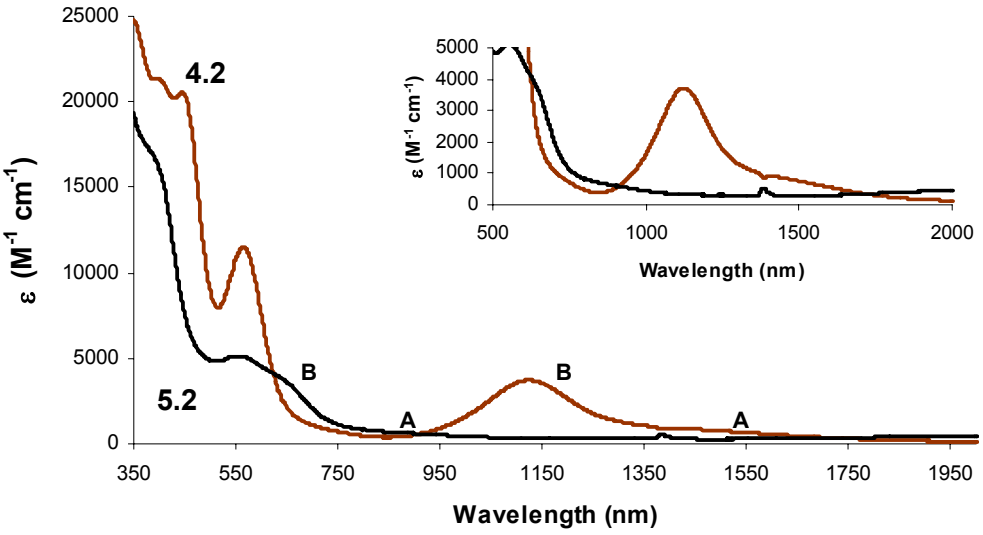

Figure 5.7. NIR data for [([PhBP$_3$]Fe)$_2$(μ-N)][Na(THF)$_5$] (**4.2**) and ([PhBP$_3$]Fe)$_2$(μ-N) (**5.2**). Potential corresponding transitions are labeled with the letters "A" and "B."

The electronic transitions of imide-hydride **5.1** were also examined with NIR spectroscopy (Figure 5.8). Although the feature at 850 nm tails off into the lower-energy regime where d-d transitions are expected, distinct ligand-field features similar to those observed for **4.2** (Figure 5.7) are not present. Consequently each metal center of **5.1** is assigned as low-spin. This is consistent with five- versus four-coordinate iron in which the presence of an additional hydride ligand contributes to a stronger ligand-field splitting in which spin pairing (versus populating strongly antibonding orbitals) is energetically favorable. This data, however, does not exclude the possibility of two exchange-coupled metal centers as a stronger ligand field may shift any observable d-d transitions to higher energy.

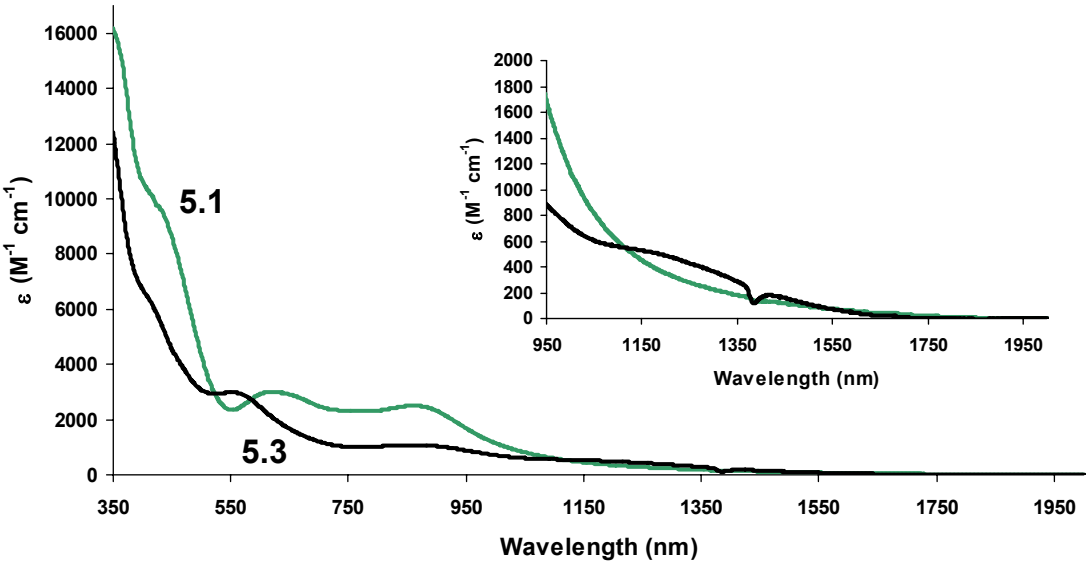

Figure 5.8. NIR data for [([PhBP$_3$]Fe)$_2$(μ-NH)(μ-H)][Na(THF)$_5$] (**5.1**), and [([PhBP$_3$]Fe)$_2$(μ-NH)(μ-H)] (**5.3**).

The reactivity patterns exhibited by neutral **5.2** resemble those of anionic **4.2**.[6] For example, exposure to an atmosphere of CO produces equimolar amounts of $[PhBP_3]Fe(CO)_2$ (**2.13**) and $[PhBP_3]Fe(NCO)(CO)_2$ (**4.4**) while hydrogenolysis with an atmosphere of H_2 at room temperature (Eq 5.1) results in the independent preparation of **5.3**. In contrast to parent **5.1**, IR spectroscopy (Nujol) of **5.3** reveals a readily discernable N-H vibration at 3319 cm^{-1}. Solid-state structural analysis has thus far been impeded by the inability to obtain crystalline samples of suitable quality for X-ray diffraction experiments.

Near-infrared analysis of **5.3** (Figure 5.8) reveals the presence of a broad transition centered at 1150 nm (ε = 540 M^{-1} cm^{-1}) that is lower in energy than any transition observed for parent **5.1**. As the ligand-field transitions of **4.2** are observed to increase in energy upon oxidation to form neutral **5.2** (Figure 5.7), this transition is assigned as an intervalence charge transfer. For comparison, it is noted that Wieghardt reported an intervalence charge-transfer transition at 866 nm (ε = 300 M^{-1} cm^{-1}) for an octahedral Fe(III)/Fe(IV) μ-nitride.[3a]

The 4 K X-band EPR spectrum of **5.3** (Figure 5.9, blue, solid line) features an axial signal attributable to an S = ½ electronic configuration. In contrast to **5.2**, a low-field signal is not observed, suggesting that at this temperature both iron centers are low spin. Delocalization of the unpaired electron over both metal centers is evidenced from weak phosphorus super-hyperfine coupling in the $g_\perp$ region, which was simulated as arising from 6 phosphorus nuclei (Figure 5.9, red, broken line, A_{6P} = 12 G).

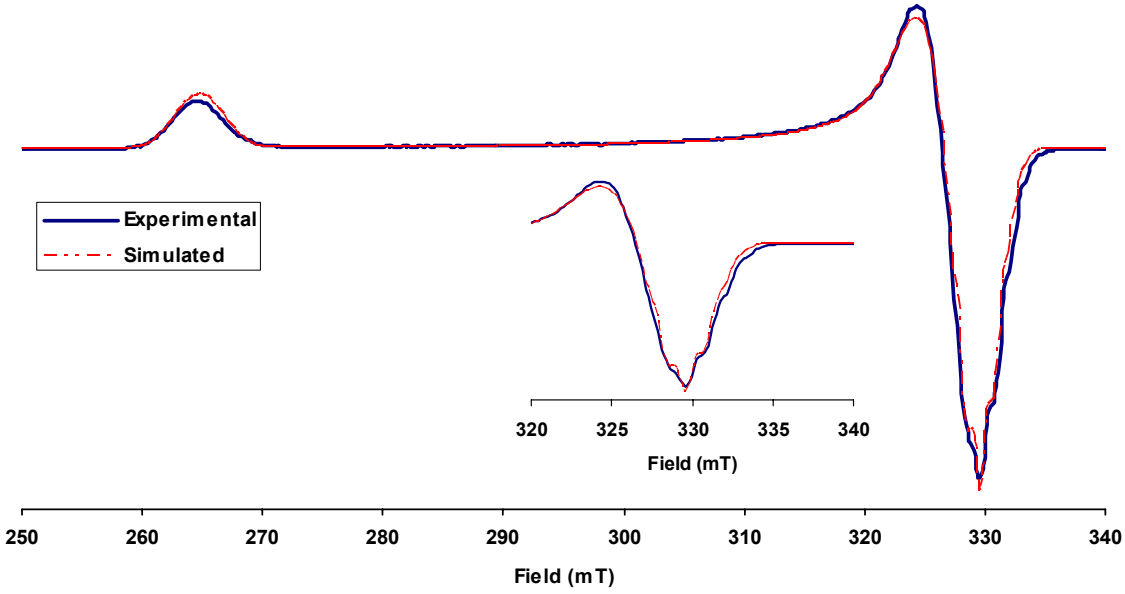

Figure 5.9. Experimental (blue, solid line) and simulated (red, broken line) X-band EPR spectrum of $([PhBP_3]Fe)_2(\mu\text{-NH})(\mu\text{-H})$ (**5.3**) (glassy toluene, 20 K, 9.374 GHz). (*inset*) Region from 320–340 mT highlighting the $g_\perp$ region. Simulation parameters: $g_1 = 2.53$, $g_2 = 2.052$, $g_3 = 2.033$; $A_{6P} = 12$ G.

Solid-state magnetic susceptibility data for **5.3** were obtained from 4 to 300 K by SQUID magnetometry and are plotted, per dimeric unit, in Figure 5.10. The plot of μ_{eff} versus temperature demonstrates that similar to **5.2**, the magnetic moment is temperature dependent and is consistent with a doublet ground state at 4 K ($\mu_{eff} = 2.12\ \mu_B$). This value increases in near linear fashion with increasing temperature and reaches a maximum of 3.30 μ_B at 300 K. As there is no evidence for antiferromagnetic coupling in the plot of χ_M versus T (not shown), this behavior likely reflects angular-momentum contributions[23] and/or the population of high-spin electronic configurations. As a final note concerning the magnetic properties of **5.3**, solution magnetic measurements (rt, Evans method) yield similar μ_{eff} values as those obtained by SQUID.

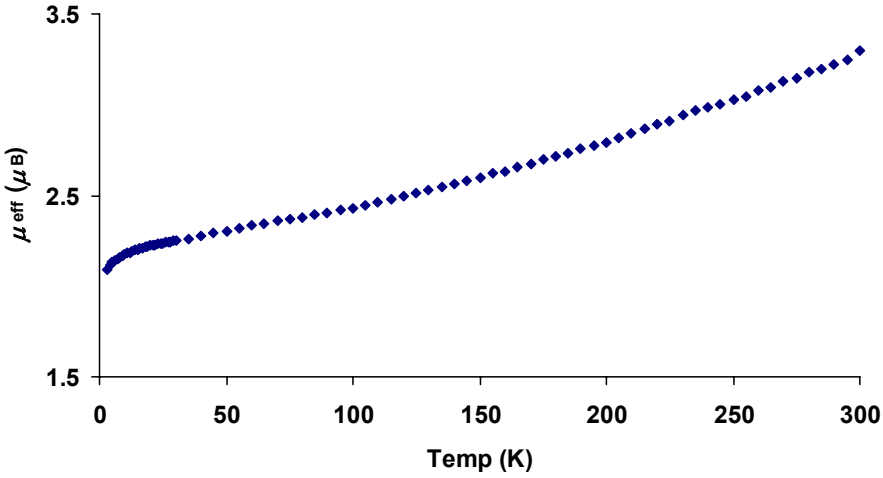

Figure 5.10. SQUID magnetometry data for ([PhBP$_3$]Fe)$_2$(μ-NH)(μ-H) (**5.3**) plotted *per dimeric unit* as μ_{eff} versus temperature.

5.3 Molecular Orbital Considerations

The iron(III) imides are characterized by one σ- and two energetically equivalent π-bonds within the Fe-N linkage, resulting in a nearly linear Fe-N-C bond angle. The molecular orbital (MO) diagram for **4.2** is of interest as the descent from C_3 to C_{2v} symmetry has significant ramifications concerning the bonding within the Fe-N-Fe manifold. To describe the bonding in **4.2**, the atomic orbitals for the nitride ligand were combined with the linear combinations of two C_{3v}-symmetric L_3Fe fragments[24] in C_{2v} symmetry (Figure 5.11). The resulting molecular orbitals reveal that the bonding within the Fe-N-Fe linkage of **4.2** is best described as 2σ + 1π, which is consistent with its bent structure. Deriving a bonding scheme for neutral **5.2** is complicated by the continued decent in symmetry as evidenced by the staggered nature of the two [PhBP$_3$] ligands.

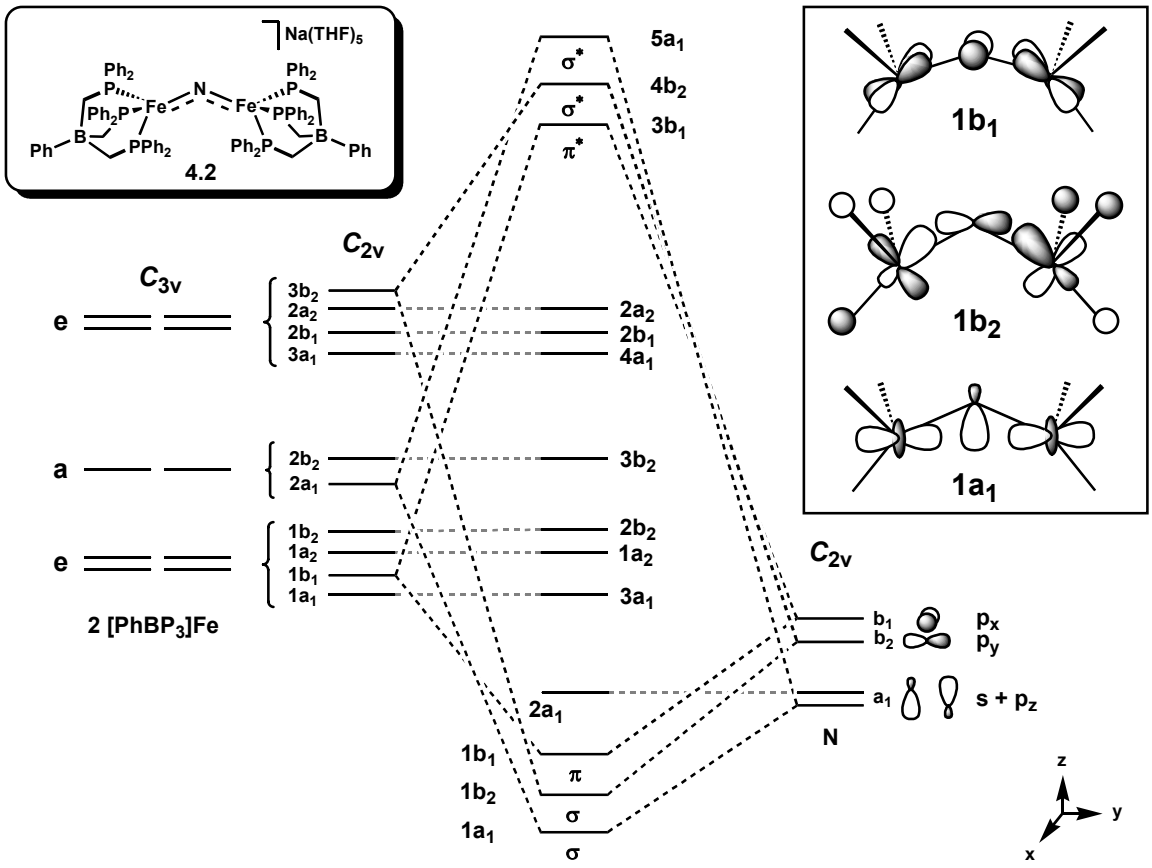

Figure 5.11. Qualitative d-orbital splitting diagram for [([PhBP$_3$]Fe)$_2$(μ-N)][Na(THF)$_5$] (**4.2**) in idealized C_{2v} symmetry. Exact orbital energies are not known.

For imide-hydride **5.1**, one of the N $p_z + s$ orbitals is involved in bonding with the H atom of the bridging-imide ligand. As shown in Figure 5.12, the imide ligand itself is linked to each iron center through 2 σ-type molecular orbitals ($2a_1$ and $1b_2$) and 1 π-bonding molecular orbital ($1b_1$). In comparison to nitride **4.2**, however, the diminished Fe-N-Fe angle in **5.3** likely minimizes orbital overlap in the $1b_2$ molecular orbital to ultimately result in the observed solid-state elongation of the Fe-N linkages. Molecular orbital $1a_1$ is also consistent with solid-state data in that it forces the imide ligand to eclipse one phenyl arm on each of the two [PhBP$_3$] ligands. For **4.2**, the iron atomic

orbitals of this parentage are bonding with respect to the nitride ligand, resulting in a staggered configuration with the two [$PhBP_3$] ligands. The addition of 20 electrons to Figure 5.12 in a low-spin configuration demonstrates that no strongly antibonding orbitals are populated. As a final comment concerning the nature of the postulated iron-iron bond, molecular orbital $2a_1$ suggests that it is in fact a 3-centered interaction.

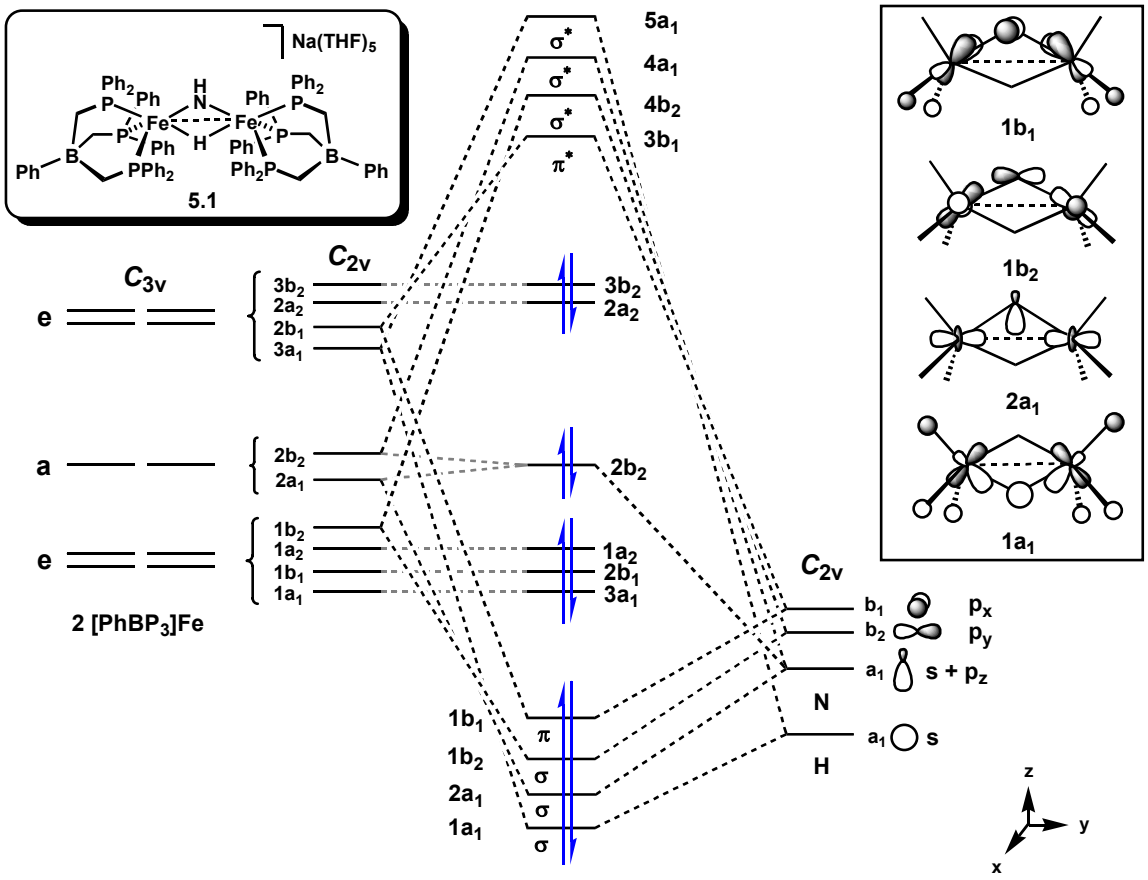

Figure 5.12. Qualitative d-orbital splitting diagram for [([$PhBP_3$]Fe)$_2$(μ-NH)(μ-H)][Na(THF)$_5$] (**5.1**) in idealized C_{2v} symmetry. Exact orbital energies are not known.

5.4 Conclusions

In summary, this work demonstrates that low-valent and low-coordinate bridging iron nitrides supported by [$PhBP_3$] are capable of facile H_2 activation under mild conditions (rt, 1 atm H_2). In contrast to earlier work concerning the hydrogenation of low-spin Fe(III) imides, complete scission of the Fe-N linkage in the present systems is not observed. This is presumably due to the presence of an additional metal center that traps a putative imide-hydride intermediate to form a bimetallic species. Spectroscopic data for both anionic **5.1** and neutral **5.3** are consistent with the presence of two low-spin d^6 iron centers. Whether related systems featuring (μ-NH) and/or (μ-H) linkages are relevant to dinitrogen reduction schemes is worth considering. Neutral **5.3**, for example, may provide spectroscopic signatures for the identification of similar species, if formed, in biologically relevant systems such as nitrogenase.[25]

5.5 Experimental Section

5.5.1 General Considerations

General considerations are outlined in Section 4.4.1.

5.5.2 Magnetic Measurements

SQUID data was acquired from 4–300 K as outlined in Section 2.5.2.

5.5.3 EPR Measurements

EPR data was acquired as outlined in Section 2.5.3.

5.5.4 Electrochemical Measurements

Electrochemical data was acquired as outlined in Section 2.5.4.

5.5.5 Starting Materials and Reagents

All reagents were purchased from commercial vendors and used without further purification unless otherwise noted. Compounds **4.2** and **4.2**-(50% ^{15}N) were prepared according to literature procedures.

5.5.6 Synthesis of Compounds

Synthesis of [([PhBP$_3$]Fe)$_2$(μ-NH)(μ-H)][Na(THF)$_5$], 5.1: [([PhBP$_3$]Fe)$_2$(μ-N)][Na(THF)$_5$] (**4.2**, 0.203 g, 0.108 mmol) was dissolved in THF (20 mL) and transferred to a 100 mL sealed flask equipped with a stirbar. The resulting brown solution was frozen in liquid nitrogen, and the N_2 atmosphere was evacuated and replaced with an atmosphere of H_2. The reaction was then allowed to warm to room temperature with stirring and within ten minutes had changed color from brown to green. After stirring for four hours at room temperature, volatiles were removed under reduced pressure, and the crude solids were washed with benzene (3 x 30 mL), petroleum ether (2 x 20 mL), and dried to yield **5.1** as a green powder (0.175 g, 86%). X-ray quality crystals were grown via a THF/hexanes vapor diffusion chamber. ^1H NMR (THF-d_8, 300 MHz): δ 18.5 (s, 1H); 7.56 (d, J = 3.0 Hz, 4H); 7.03 (t, J = 7.2 Hz, 4H); 6.90 (m, 26H); 6.80 (t, J = 7.8 Hz, 12H); 6.56 (t, J = 7.8 Hz, 24H); 3.60 (m, 20H); 1.78 (m, 20H); 1.31 (br s, 12H). $^{31}P\{^1H\}$ NMR (THF-d_8, 121.4 MHz): δ 66.0 (s). Anal. Calcd. for $C_{110}H_{124}B_2Fe_2NNa0_5P_6$: C, 70.19; H, 6.64; N, 0.74 Found: C, 69.82; H, 6.50; N, 0.83. For the ^{15}N NMR data, a sample of **4.2**-(50% ^{15}N) was hydrogenated in a J. Young tube. ^{15}N NMR (THF, 50.751 MHz): δ 406 (d, $^1J_{N\text{-}H}$ = 63 Hz). ^1H NMR (THF-d_8, 300 MHz): δ 18.5 (virtual triplet due to the 50% ^{14}NH singlet and the 50% ^{15}NH doublet ($^1J_{N\text{-}H}$ = 63 Hz), 1H).

Synthesis of ([PhBP$_3$]Fe)$_2$(μ-N), 5.2: [([PhBP$_3$]Fe)$_2$(μ-N)][Na(THF)$_5$] (**4.2**, 0.300 g, 0.160 mmol) was dissolved in THF (20 mL) with stirring. A THF solution (5 mL) of PCl_3 (14 μL, 0.160 mmol) was added dropwise, which resulted in a rapid darkening of the reaction solution. After 2 hours volatiles were removed under reduced pressure, and the crude solids were extracted with benzene (50 mL), filtered over Celite, and lyophilized. The resulting solids were washed with Et_2O (2 x 20 mL) and dried to obtain **5.2** as a dark solid (0.157 g, 66%). X-ray quality crystals were grown via vapor diffusion of petroleum ether into a THF solution. ^{1}H NMR (C_6D_6, 300 MHz): δ 52.5 (s); 19.7 (s); 12.6 (s); 11.5 (t, J = 6.0 Hz); 6.14 (d, J = 6.0 Hz); -1.69 (s); -6.44 (s). μ_{eff} = 3.40 μ_B at 300 K (SQUID). Anal. Calcd. for $C_{90}H_{82}B_2Fe_2NP_6$: C, 72.22; H, 5.52; N, 0.94 Found: C, 71.92; H, 5.56; N, 0.74.

Synthesis of ([PhBP$_3$]Fe)$_2$(μ-NH)(μ-H), 5.3: [([PhBP$_3$]Fe)$_2$(μ-NH)(μ-H)][Na(THF)$_5$] (**5.1**, 0.400 g, 0.213 mmol) was dissolved in THF (40 mL) with stirring. Solid [NO][BF_4] (0.0248 g, 0.213 mmol) was added to this solution in one portion. The green color of **5.1** gradually fades and after two hours volatiles were removed under reduced pressure and the crude solids were extracted with benzene (~ 80 mL), filtered over Celite, and lyophilized. The resulting solids were washed with Et_2O (2 x 20 mL) and dried to obtain **5.3** as a dark solid (0.248 g, 78%). ^{1}H NMR (THF-d_8, 300 MHz): δ 21.4 (v br, s); 11.9 (s); 9.00 (s); 8.51 (t, J = 6.3 Hz); 7.11 (s); 3.53 (s, overlaps with residual solvent resonance); 1.03 (br, s). μ_{eff} = 3.13 μ_B at 300 K (SQUID). IR (Nujol): ν_{NH} = 3319 cm^{-1}. Anal. Calcd. for $C_{90}H_{84}B_2Fe_2NP_6$: C, 72.12; H, 5.65; N, 0.93 Found: C, 71.73; H, 5.76; N, 0.80.

5.5.7 X-ray Experimental Data

Crystallographic procedures are outlined in Section 2.5.8. Crystallographic data are summarized in Table 5.2.

Table 5.2. Crystallographic data for $[([PhBP_3]Fe)_2(\mu\text{-}NH)(\mu\text{-}H)][Na(THF)_5]$ (**5.1**) and $([PhBP_3]Fe)_2(\mu\text{-}N)$ (**5.2**).

	5.1	**5.2**·2 THF
chemical formula	$C_{110}H_{124}B_2Fe_2NNaO_5P_6$	$C_{98}H_{98}B_2Fe_2NO_2P_6$
fw	1882.23	1640.91
T (°C)	-177	-177
λ (Å)	0.71073	0.71073
a (Å)	13.712(2)	23.519(5)
b (Å)	23.001(4)	13.524(3)
c (Å)	30.221(5)	25.937(6)
α (°)	90	90
β (°)	91.006(6)	95.178(4)
γ (°)	90	90
V (Å^3)	9530(3)	9965.8(8)
space group	P2(1)/c	P2(1)/n
Z	4	4
D_{calc} (g/cm^3)	1.312	1.327
μ(cm^{-1})	4.66	5.22
R1, wR2[a] ($I > 2\sigma(I)$)	0.0666, 0.0941	0.0501, 0.0726

[a] $R1 = \Sigma||F_o| - |F_c||/\Sigma|F_o|$, $wR2 = \{\Sigma[w(F_o^2 - F_c^2)^2]/\Sigma[w(F_o^2)^2]\}^{1/2}$

References Cited

[1] Ertl, G. *Chem. Rec.* **2001**, *1*, 33.

[2] (a) Betley, T. A.; Peters, J. C. *J. Am. Chem. Soc.* **2004**, *126*, 6252. (b) Meyer, K. M.; Eckhard, B.; Mienert, B.; Weyhermuller, T.; Wieghardt, K. *J. Am. Chem. Soc.* **1999**, *121*, 4859. (c) Wagner, W.-D.; Nakamoto, K. *J. Am. Chem. Soc.* **1989**, *111*, 1590.

[3] (a) Justel, T.; Muller, M.; Weyhermuller, T.; Kressl, C.; Bill, E.; Hildebrandt, P.; Lengen, M.; Grodzicki, M.; Trautwein, A. X.; Nuber, B.; Wieghardt, K. *Chem.-Eur. J.* **1999**, *5*, 793. (b) Kienast, A.; Homborg, H. *Z. Anorg. Allg. Chem.* **1998**, *624*, 233. (c) Moubaraki, B.; Benlian, D.; Baldy, A.; Pierrot, M. *Acta Crystallogr., Sect. C* **1989**, *45*, 393. (d) Scheidt, W. R.; Summerville, D. A.; Cohen, I. A. *J. Am. Chem. Soc.* **1976**, *98*, 6623. (e) Summerville, D. A.; Cohen, I. A. *J. Am. Chem. Soc.* **1976**, *98*, 1747.

[4] For ammonia production from a terminal iron nitride with hydrogen equivalents see reference [2a].

[5] Brown, S. D.; Peters, J. C. *J. Am. Chem. Soc.* **2004,** *126,* 4538.

[6] Brown, S. D.; Peters, J. C. *J. Am. Chem. Soc.* **2005,** *127,* 1913.

[7] For $(Cp_2Ti)_2(\mu\text{-}NH)_2(\mu\text{-}H)$ see: Armor, J. N. *Inorg. Chem.* **1978,** *17,* 203.

[8] For examples of bimetallic systems featuring μ-NH ligands see: (a) Wraage, K.; Schmidt, H.-G.; Noltemeyer, M.; Roesky, H. W. *Eur. J. Inorg. Chem.* **1999,** 863. (b) Puff, H.; Hanssgen, D.; Beckermann, N.; Roloff, A.; Schuh, W. *J. Organomet. Chem.* **1989,** *373,* 37. (c) Edelblut, A. W.; Haymore, B. L.; Wentworth, R. A. D. *J. Am. Chem. Soc.* **1978,** *100,* 2250. (d) Abarca, A.; Martin, A.; Mena, M.; Yelamos, C. *Angew. Chem., Int. Ed.* **2000,** *39,* 3460.

[9] Roesky, H. W.; Bai, Y.; Noltemeyer, M; *Angew. Chem., Int. Ed.* **1989,** *28,* 754.

[10] Daida, E. J.; Peters, J. C. *Inorg. Chem.* **2004,** *43,* 7474.

[11] See for example: (a) Georgakaki, I. P.; Miller, M. L.; Darensbourg, M. Y. *Inorg. Chem.* **2003,** *42,* 2489. (b) Zhao, X.; Chiang, C.-Y.; Miller, M. L.; Rampersad, M. V.; Darensbourg, M. Y. *J. Am. Chem. Soc.* **2003,** *125,* 518 and references therein. (c) Gloaguen, F.; Lawrence, J. D.; Rauchfuss, T. B.; Bénard, M.; Rohmer, M.-M. *Inorg. Chem.* **2002,** *41,* 6573. (d) Lawrence, J. D.; Rauchfuss, T. B.; Wilson, S. R. *Inorg. Chem.* **2002,** *41,* 6193.

[12] The cyclic voltammagram of $[NBu_4][BPh_4]$ in CH_2Cl_2 features an irreversible oxidation at ~ 0.75 V vs. S.C.E. (~ 0.26 V vs. Fc/Fc^+). For complete experimental details see: Pal, P. K.; Chowdhury, S.; Drew, M. G. B.; Datta, D. *New J. Chem.* **2002,** *26,* 367.

[13] Orpen, A. G.; Connelly, N. G. *Organometallics* **1990,** *9,* 1206.

[14] A similar phenomenon has been observed for the complex $[(PP_3)Fe(C{\equiv}CPh)][BPh_4]$ (PP_3 = $P(CH_2CH_2PPh_2)_3$). The one-electron reduction of this species induced a contraction of the Fe-P bond distances by an average of 0.09 Å, which the authors attributed to π-backbonding. See: Bianchini, C.; Laschi, F.; Masi, D.; Ottaviani, F. M.; Pastor, A.; Peruzzini, M.; Zanello, P.; Zanobini, F. *J. Am. Chem. Soc.* **1993,** *115,* 2723.

[15] For EPR analysis of the d^5 iron imides see Chapter 2. Also see: Brown, S. D.; Peters, J. C. *J. Am. Chem. Soc.* **2003,** *125,* 322.

[16] For antiferromagnetic coupling between $S_1 = 5/2$ and $S_2 = 2$ centers, the S = 3/2 spin state is expected to lie 3*J* higher in energy than the S = ½ spin state. See: Kurtz, D. M., Jr. *Chem. Rev.* **1990,** *90,* 585.

[17] For examples of χ_M and μ_{eff} vs. T plots obtained for antiferromagnetically coupled Fe(II)/Fe(II) systems, see: Klose, A.; Solari, E.; Floriani, C.; Chiese-Villa, A.; Rizzoli, C.; Re, N. *J. Am. Chem. Soc.* **1994,** *116,* 9123.

[18] (a) Hay, P. J.; Thibeault, J. C.; Hoffmann, R. *J. Am. Chem. Soc.* **1975,** *97,* 4884 and references therein. (b) Murray, K. S. *Coord. Chem. Rev.* **1974,** *12,* 1.

[19] See for example: (a) Mukherjee, R. N.; Stack, T. D. P.; Holm, R. H. *J. Am. Chem. Soc.* **1988,** *110,* 1850. (b) Drew, M. G. B.; McKee, V.; Nelson, S. M. *J. Chem. Soc., Dalton Trans.* **1978,** 80.

[20] See for example: (a) Norman, R. E.; Holz, R. C.; Menage, S.; O'Connor, C. J.; Zhang, J. H.; Que, L., Jr. *Inorg. Chem.* **1990,** *29,* 4629. (b)Mabbs, F. E.; McLachlan, V. N.; McFadden, D.; McPhail, A. T. *J. Chem. Soc., Dalton Trans.* **1973,** 2016.

[21] Examples of C_1 symmetric, μ-oxo iron species are known in which the coupling is *stronger* than in related C_{2v} systems. See for example: Gomez-Romero, P.; Witten, E. H.; Reiff, W. M.; Jameson, G. B. *Inorg. Chem.* **1990,** *29,* 5211.

[22] For example, Δ_{oct} for $Co(NH_3)_6^{3+}$ and $Co(NH_3)_6^{2+}$ are 22,900 and 10,200 cm^{-1}, respectively. See: Housecroft, C. E.; Sharpe, A. G. *Inorganic Chemistry;* 2nd Ed., Pearson Education Limited: England, 2005; p 559.

[23] Octahedral Fe(III) compounds with low-spin t_{2g}^5 configurations have considerable orbital contributions to their magnetic moments, which are therefore intrinsically temperature dependent. Cotton, F. A.; Wilkinson, G.; Murillo, C. A.; Bochman, M. *Advanced Inorganic Chemistry;* 6th Ed., Wiley & Sons: New York, 1999; p 790.

[24] Albright, T. A.; Burdett, J. K.; Whangbo, M.-H. *Orbital Interactions in Chemistry;* Wiley & Sons: New York, 1985; p 383.

[25] See for example: Igarashi, R. Y; Laryukhin, M.; Dos Santos, P. C.; Lee, H.-L.; Dean, D. R.; Seefeldt, L. C.; Hoffman, B. M. *J. Am. Chem. Soc.* **2005,** *127,* 6231.